

# Geochemical Characteristics of the Granitic Rocks at Magal Gebriel Area, South Eastern Desert, Egypt

Gehan B. El Shaib<sup>1</sup>, Adel H. El Afandy<sup>1</sup>, Nasser M. Moghazy<sup>1</sup> and Atef El-TaHER<sup>2</sup>

<sup>1</sup>Nuclear Materials Authority, P.O. 530, El-Maadi, Cairo, Egypt.

<sup>2</sup>Physics Department, Faculty of Science, Al-Azhar University, Assuit Branch, 71524, Assuit, Egypt.

Received: 28 Feb. 2023, Revised: 12 Mar. 2023, Accepted: 22 Mar. 2023.

Published online: 1 May 2023.

**Abstract:** The study area comprises volcano sedimentary succession (metasediment and metavolcanics) intruded by granitoid rocks. The younger granites occupy central, northeastern and northwestern parts of the area, they form moderate to high outcrops and have sharp intrusive contacts with the surrounding metavolcanics. These rocks are highly jointed and affected by hydrothermal alterations, especially along faults and shear zones. The studied syeno- and alkali feldspar granites were investigated by polarized microscopes, analyzed for trace and rare earth element by X-ray fluorescence, ICP-ES and ICP-MS techniques. Petrographically, Syeno- and alkali feldspar granites are mainly composed of quartz, alkali feldspar, plagioclase, biotite and muscovite as essential minerals, fluorite, zircon, allanite, titanite, monazite, uranophane and iron oxides as accessories. The present study focus on the geochemical characteristics investigation of syeno- and alkali feldspar granites at Magal Gebriel area to detect their suitability for radionuclides and other mineralization. All samples of the alkali feldspar and syenogranite samples have La/Y ratios  $< 1$ , suggesting the prevailing of acidic conditions in the depositional environment. REEs mobility are mainly controlled by the pH conditions of the media, therefore, the migration out of REEs is higher in the alkali feldspar granite relative to syenogranites. Ce anomalies in the most alkali feldspar and syenogranite samples ( $< 1$ ) and have negative Eu anomalies, indicating its formation under reducing conditions by hypogene hydrothermal fluids, having temperature  $> 200^{\circ}\text{C}$ , low pH, and relatively high  $f\text{O}_2$ . The nonchondritic values of isovalues, illustrating the dual impact of hydrothermal solution and water on the alteration processes of these rocks. Late alteration processes lead to increments and decrements in some elements and formation of new minerals. The conjugate M-W tetrad effect in the alkali feldspar granite emphasize the alteration processes and may clarify the presence of gold mineralization.

**Keywords:** Radiation detector, Silicon drift detector, SiPM, Scintillator, Gamma ray detector, X-ray, Spectrometer.

## 1 Introduction

The abundance of these post-orogenic granites is of geodynamic interest, as they represent a significant addition of material into the juvenile crust of the Arabian-Nubian Shield (ANS) over a relatively short time interval. These highly-fractionated granites and associated pegmatites, also, host important mineral deposits, with anomalously elevated concentrations of critical elements including Li, Be, F, Zr, Nb, Mo, Sn, Ta, W, Pb, Th, U, and rare earth elements (REEs) [1, 2]. In the Eastern Desert of Egypt, these granites are called rare-metal granites.

The U-rich igneous rocks are considered as a significant source of metals in U mineral systems. The relationship is manifested by the wide spatial correlation between known U deposits and igneous rocks containing

high abundances of U [3]. Generally, U is initially mobilized from igneous rocks by hydrothermal and/or surficial fluids [4,5], whereas U deposits resulting only from the magmatic process (partial melting or fractional crystallization) are rare [6].

The Magal Gebriel area is located in the south Eastern Desert of Egypt about 170 Km southeast Aswan, between latitudes  $22^{\circ} 51'$  and  $22^{\circ} 58'$  N and longitudes  $33^{\circ} 35'$  and  $33^{\circ} 44'$  E covers about  $235 \text{ Km}^2$  (Fig. 1).

The field geology, structure, petrology, mineralogy, radioactivity, geochemistry and geochronology of the investigated area were studied by [7:12].

The increasing-decreasing trends for most trace elements in various geologic environments is related to the variations in physico-chemical conditions of the fluids such

\* Corresponding author e-mail:

as pH, Eh, temperature, and ionic complexes during the development of this deposit [13]. Though, the high field strength elements (HFSE) like Zr, Ga, Hf, and Th are considered immobile during the alteration processes [14] they show both increasing and decreasing trends during the development of the Mortas- bauxite deposit [15]. This dual behavior for these elements can be attributed to factors such as low pH, intensity of alteration, high water-rock ratios, and abundance of complex-making ions like  $\text{CO}_3^{2-}$ ,  $\text{F}^-$ ,  $\text{Cl}^-$ ,  $\text{PO}_3^{4-}$ , and  $\text{SO}_4^{2-}$  in hydrothermal solutions played an important role in leaching of these elements out of the system [16]. [17] revealed that high-temperature altering fluids cause mobility of HFSE and brings about the exit of Zr and Y from the alteration system while the low-temperature fluids induced enrichment of these elements.

Generally, it is illustrated that REE show low mobility and are resistant to fractionation during weathering processes in surficial environments, some authors advocate that mobilization and fractionation may occur in different stages of weathering (e.g., [18, 19,20]. Radius and charge are mainly controlled REE behavior (CHARAC); therefore, normalized REE patterns versus atomic number curves are smooth [21]. In some cases, irregular shapes of the normalized patterns could be attributed to the tetrad effect. This phenomenon has been firstly recorded for liquid-liquid systems of organic ligands in the 1960 [22, 23]. Many researchers reported the tetrad effect of lanthanides for various rock types and different geological environments and used it as an indicator of REE fractionation [24:30]. Four distinct groups (tetrads) in normalized REE patterns were distinguished: the first from La to Nd, the second from Pm to Gd, the third from Gd to Ho, and the fourth from Er to Lu [26]. Note that Gd is included in both the second and third tetrads. The divisions represent one-fourth, one-half, three-fourths, and filled 4f orbital of the lanthanides [31]. Previous studies have shown that phosphate minerals such as apatite, fluor-apatite and monazite can be used to evaluate REE fractionation during geochemical processes, because these minerals are assumed to be the source of the REE and are common as accessory minerals in various geological environments [32:37].

The present study focus on the geochemical characteristics investigation of younger granite varieties (syeno- and alkali feldspar granites) at Magal Gebriel area to detect their suitability for radionuclides and other mineralization.

## 2 Geologic setting

The area comprises igneous and metamorphic rocks which are represented by a low grade metamorphosed volcano-sedimentary succession intruded by granitoid rocks (Fig.1). The metasediments are the oldest rock unit in the study area and crop out in the southwestern part of the mapped area as isolated masses. They form low to moderate relief masses of greyish green colour and are invaded by the metavolcanics and granites. They comprise biotite schist, chlorite schist, quartz-feldspathic schist and have mainly NW-SE trending foliation.

The *metavolcanics* crop out in the central and eastern parts of the study area as an elongated belt trending NW-SE, forming low to moderate relief. They are represented by metabasalt, meta-andesite and metarhyolite as younger metavolcanics which are intruded by syenogranites commonly with sharp intrusive contacts (Fig. 2a). *Granitoid* rocks including older and younger varieties. The older variety composed mainly of diorites-granodiorites rock types. They intruded by syenogranites. These rocks have xenoliths of metavolcanics. They are of limited distribution and found as low hills restricted in the northern part of the area, with greyish to pale reddish color and medium to coarse-grained. The younger granites occupy both the central, northeastern and northwestern parts of the mapped area as a medium to coarse-grained syenogranites and fine grained alkali feldspar granites. They form moderate to high outcrops and have sharp intrusive contacts with the surrounding metavolcanics (Fig. 2b).

These rocks are highly jointed and characterized by exfoliation weathering and bouldary appearance (Fig. 2b, c & d). The field studies indicated that these granites are affected by hydrothermal alterations, especially along faults and shear zones. The field radiometric survey revealed high intensity of radioactivity in the alkali feldspar granite especially in hematitized and kaolinized zones of the granites mainly along the intersect fracture planes trending NE and NW directions. The area is dissected by a series of faults commonly trending in the NE-SW, NW-SE, ENE-WSW, NNE-SSW and E-W directions.

## 3 Methodologies

Fifty five representative samples were collected and fifteen of them were chosen from syeno- and alkali feldspar granites, these samples were prepared as thin

sections and examined under a polarizing microscope to determine their texture and mineralogical composition.

Nineteen representative samples were selected for, trace and REE elements analyses at the Acme Laboratory, Canada. Samples were crushed and then powdered using agate mortar to avoid trace elements contamination and are prepared for complete chemical analysis.

#### 4 Petrography

**Syenogranite** is abundant in the north of Magal Gebreil area and composed of quartz alkali feldspar, plagioclases, biotite and muscovite. Zircon, apatite, iron oxides, monazite, allanite and titanite are the accessory minerals. Quartz is present in clusters and isolated with regular boundaries, and also consertal texture, intergrowth texture either graphic or myrmekitic texture are present. Strained and undulatory extinction in addition to wavy extinction is also recorded. Potash feldspar is the most dominant feldspar in the rock and is represented mainly by orthoclase perthite, microcline perthite and microcline, occurs as large subhedral to anhedral crystals partially altered to sericite or kaolinite (Fig. 3a, b & c).

Plagioclases (mainly albite and oligoclase) are present with lamellar twinning and minute inclusions of quartz (Fig.3c). Biotite is the most ferromagnesian mineral, with pleochroic haloes resulting from the presence of radioactive zircon, altered to epidote, chlorite, and muscovite (Fig. 3e, f & g). Muscovite is rarely essential minerals but occurs as alteration product of potash feldspar and /or biotite (Fig 3h).

**Alkali feldspar granite** is abundant around Gabal Magal Gebreil with fine to medium-grained rock samples and composed mainly of quartz, alkali feldspar, plagioclase, biotite and muscovite as essential minerals. Garnet, Fluorite, zircon, allanite, titanite, monazite, uranophane and iron oxides as accessories (Fig. 4a, b, c, d & f). Quartz is medium-grained, independent in some samples and has intergrowth relationship with alkali feldspar and plagioclase. Alkali feldspars are mainly microcline with cross-hatched twinning and also involved in perthitic texture, enclosing quartz, plagioclase, muscovite. Plagioclase (albite) is subhedral crystals, isolated crystals or involved in intergrowth textures, altered to saussurite, zoned crystals and corroded due to alteration effect.

Muscovite is abundant in most of these samples as essential mineral and some as an alteration product.

Biotite is absent in some samples whereas present in the others as ferromagnesian mineral (annite) (Fig. 4e). Generally, uranophane is stained with a thin crust of hematite (Fig. 4d). This may be due to the ability of iron oxides to adsorb uranium from circulating solutions or due to the prevalence of oxidation conditions that cause the precipitation of uranium as  $U^{6+}$ . However, [38] concluded that hematitization is formed as minor alteration phase during the alteration of biotite. [39] suggested that the hematitization process is related to alkaline solution at pH

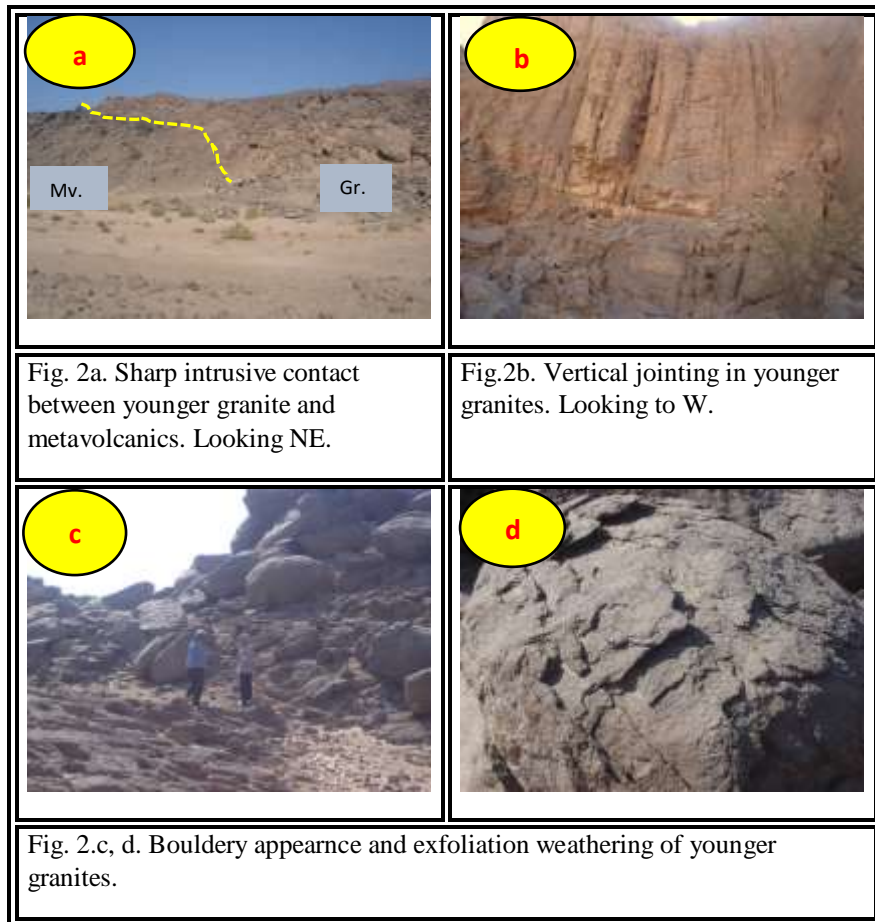
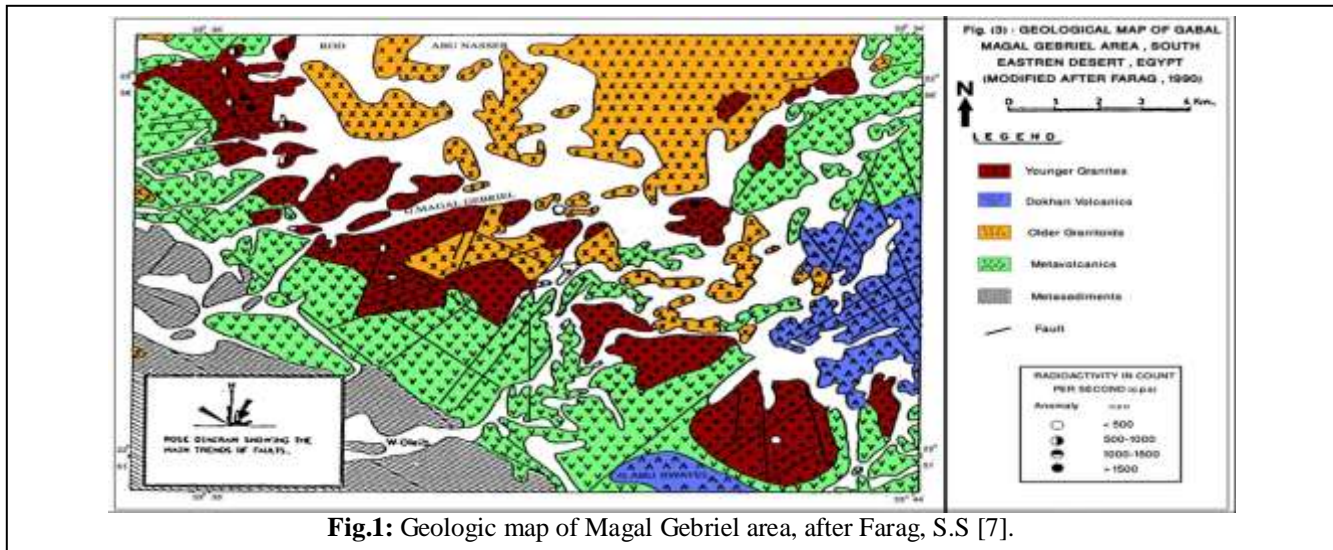
value  $>10$  and temperature ranging between  $350\text{--}500^\circ\text{C}$ .






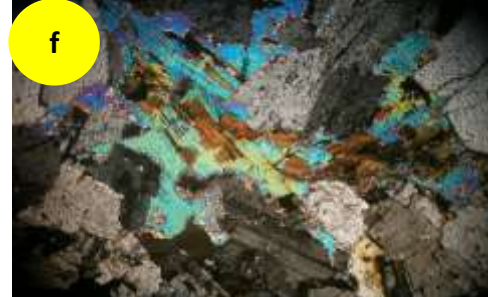


In kaolinized granite, the feldspars are completely altered to kaoline giving quartz and  $K^+$ . The liberated  $K^+$  into solution alter the plagioclase to clay minerals and quartz and the rock becomes light in color and more brittle. Sericitized granite is distinguished by transformation of plagioclase and K-feldspar to sericite and amorphous silica (Fig. 3b) with disappearance of the original texture. Biotite in the sericitized granite is altered to chlorite which characterized by low to moderate pleochroism and ranges in color from pale green to dark green.

Titanite occurs either as primary euhedral crystals characterized by wedge shape or as secondary anhedral crystals associated with opaque minerals (Fig. 4c). Secondary uranium minerals as uranophane is stained with a thin crust of hematite (Fig. 4d). This may be due to the ability of iron oxides to adsorb uranium from circulating solutions or due to the prevalence of oxidation conditions that cause the precipitation of uranium as  $U^{6+}$ . Secondary uranium minerals may be adsorbed within mica (annite) or occur as fracture filling within fractured opaques (Fig. 4e & f).

However, [38] concluded that hematitization is formed as minor alteration phase during the alteration of biotite. [39] suggested that the hematitization process is related to alkaline solution at pH value  $>10$  and temperature ranging between  $350\text{--}500^\circ\text{C}$ .

In kaolinized granite, the feldspars are completely altered to kaoline giving quartz and  $K^+$ . The liberated  $K^+$  into solution starts to alter the plagioclase to clay minerals and quartz and the rock becomes light in color and more brittle. Sericitized granite is distinguished by transformation of plagioclase and K-feldspar to sericite and amorphous silica (Fig. 3b) with disappearance of the original texture. Biotite in the sericitized granite is altered to chlorite which characterized by low to moderate pleochroism and ranges in color from pale green to dark green.



	
<p>Fig.3a. Microcline perthite showing cross-hatching and corroded with plagioclase laths along preperies . C.N., x40.</p>	<p>Fig.3b. Intensive sericitization of perthite crystal engulfing secondary quartz crystal and plagioclase laths. C.N., x20.</p>
	
<p>Fig.3c. Monazite crystal (Mo.) engulfed within plagioclase laths, while zircon crystal (Zr.) coated by iron oxides within silica. C.N., X40.</p>	<p>Fig.3d Fluorite with muscovite associating opaque radioactive mineral engulfed within perthite crystal.C.N., X40.</p>
	
<p>Fig.3e. Titanite with euhedral hematized core allanite crystal and associating biotite flake. C.N., x40.</p>	<p>Fig. 3f. Phlogopite spatially altered to biotite. C.N., X40.</p>
	
<p>Fig.3g. Muscovitization of biotite flakes along peripheries.C.N., x40.</p>	<p>Fig.3h. Partial muscovitization of biotite with iron oxides enrichment. C.N. x40.</p>

## 5 Geochemistry

Nineteen bulk rock samples of the studied granites (9 samples from syenogranite, 10 samples from alkali feldspar granite) were analyzed for major oxides, trace and rare earth elements in Acme Analytical Laboratories, Canada. The major oxides, trace elements and calculated CIPW norm calculation are registered in Table. 1.

### Geochemical characteristics of the studied granites:

The loss and gain of elements causes geochemical changes in major and trace elements. According to [40], normalizing altered granites on the upper continental crust (UCC) is advised for understanding the geochemical behavior of major, trace elements in the studied granites. Afterward, the reference UCC becomes flat at unity, and the relative depletion or enrichment is given by the deviations on both sides of the reference line (Fig.5& 6).

Geochemistry of major elements is discussed in terms of gains (positive) and losses (negative) of these elements during granite alteration. The altered alkalifeldspar and syenogranite samples show an increase in  $\text{SiO}_2$ ,  $\text{Na}_2\text{O}$ ,  $\text{K}_2\text{O}$ , in addition to a noticeable decrease in  $\text{Al}_2\text{O}_3$ ,  $\text{Fe}_2\text{O}_3$ ,  $\text{MgO}$ ,  $\text{CaO}$ ,  $\text{TiO}_2$ , and  $\text{P}_2\text{O}_5$  in all samples.

Enrichment in  $\text{SiO}_2$  may be correlated with the silicification processes, as indicated from petrographic studies and can be due to the considerable quantity of free Si-bearing mineral phases (e.g., quartz) that increase in the more evolved granites. The silicification process leads to silica enrichment at the expense of other major oxides. The enrichment of Na, and K in all samples (Fig.5) could be related alkali metasomatism of these rocks. The loss of Mg in all of the studied samples may result from the destruction and alteration of ferromagnesian minerals. Depletion of Ti may be related to the destruction of biotite by hypogene solutions, while the diminution of P is in connection with destruction of apatite.

The presence of enrichment-depletion trends for minor elements (Fig.6) is due to the variations of the physico-chemical conditions of the fluids, such as the pH, Eh, temperature, and ionic complexes during the development of this deposit [41]. Abundances of trace elements in the hydrothermally altered alkalifeldspar granite samples are either higher (Hf, Nb, Rb, Ta, Th, U, Zr, Pb and Y) or lower (Ba, Ga and Zn), while syenogranites exhibit enrichment in Nb, Ba, Ta, Th, U, Pb and Y but depleted in Hf, Rb, Zr and Zn than those in the upper continental crust.

Rb, , and Ga increase with increasing sericite clay minerals due to the sericitization processes, which could be relates to Ba diminution. It was suggested that Rb concentrations increased in a liquid-rich phase.

While zirconium enrichment in the alkalifeldspar granites may be connected zircon abundance as clarified from petrographic investigations. On the other hand, syenogranites showed reduction in its contents compared with that of alkalifeldspar granites, this rarity could be related to zircon fractionation, since it is an early crystallized mineral. High U, Nb, Y, Th and Pb contents may be controlled by the presence of uranophane, thorite, allanite zircon, fluorite and titanite.

### Environment of deposition.

#### La/Y ratios.

La/Y ratios lesser than unity are an indication of acidic environment while values higher than unity clarified alkalic environment [42, 43, 30]. All samples of the alkali feldspar and syenogranite samples have La/Y ratios  $<1$  suggesting the prevailing of acidic conditions in the depositional environment. REEs mobility are mainly controlled by the pH conditions of the media [32]. REEs are highly mobilized under acidic conditions of weathering products, while they are precipitated under neutral to alkaline conditions [44, 30]. This may be confirmed by the low values of the total rare earth elements in the alkali feldspar and syenogranite relative to non-altered granite (250-270 ppm) [45]. REEs are highly mobilized under the acidic conditions of weathering products, while they are precipitated under neutral-to-alkaline conditions [30].

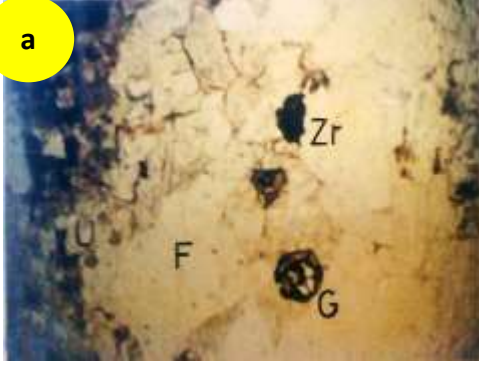


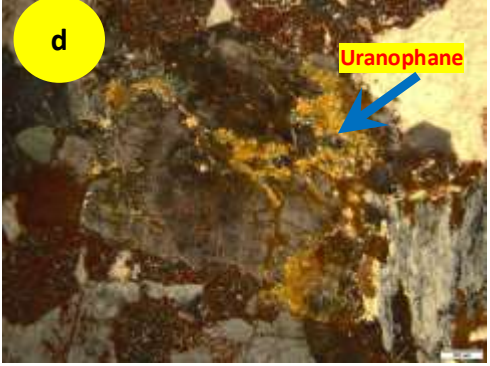

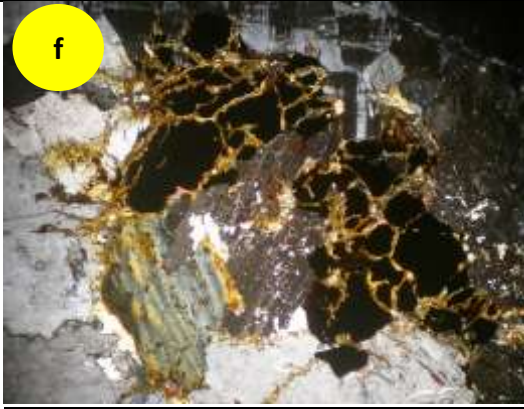
#### Oxidation-Reduction conditions.

#### Ce and Eu anomaly.

Ce anomaly is strongly controlled by by the fugacity of oxygen during geochemical processes [46]. Oxidizing environments causes  $\text{Ce}^{3+}$  to be converted into  $\text{Ce}^{4+}$  with smaller ionic radii and higher charge [47]. Ce in a tetravalent oxidation state is generally much less mobile relative to other  $\text{REE}^{3+}$  [48]. This means that under oxidation conditions  $\text{Ce}^{4+}$  increase in the sediments and causes positive anomaly [49]. In contrast, in reducing conditions the more soluble  $\text{Ce}^{3+}$  will be dominant causing a negative Ce anomaly in sediments [50]. Ce anomalies in the most alkali feldspar and syenogranite samples ( $< 1$ ) suggesting its formation under reducing conditions.

Eu, is an oxidation-sensitive element. It has two oxidation states ( $\text{Eu}^{2+}$  and  $\text{Eu}^{3+}$ ) during geochemical processes. Eu-bearing minerals solubility (feldspars) during hydrothermal alterations will mobilize Eu into solutions/fluids which is strongly mobile, and reduction of

$\text{Eu}^{3+}$  to  $\text{Eu}^{2+}$  can occur at temperatures  $>200^\circ\text{C}$  [51]. All the alkalifeldspar and syenogranite samples have negative Eu anomalies. Negative Eu anomalies may be controlled by hypogene hydrothermal fluids, having temperature  $>200^\circ\text{C}$ , low pH, and relatively high  $f\text{O}_2$ .

	
<p>Fig.4a Fluorite with muscovite associating opaque radioactive mineral engulfed within perthite crystal.PPL.X 20</p>	<p>Fig.4b. A metamict zircon crystal on the border between biotite and quartz . C.N. X40.</p>
	
<p>Fig.4c. Euhedral crystal of titanite engulfed within quartz. C.N. X40.</p>	<p>Fig.4d. uranophane crystal associating subhedral plagioclase laths coated with iron oxides. C.N. x20</p>
	
<p>Fig.4e. Annite crystal rich in radioactive nuclei.C.N. X40.</p>	<p>Fig.4f. Fractured opaques associations with secondary radioactive minerals. C.N. X40.</p>



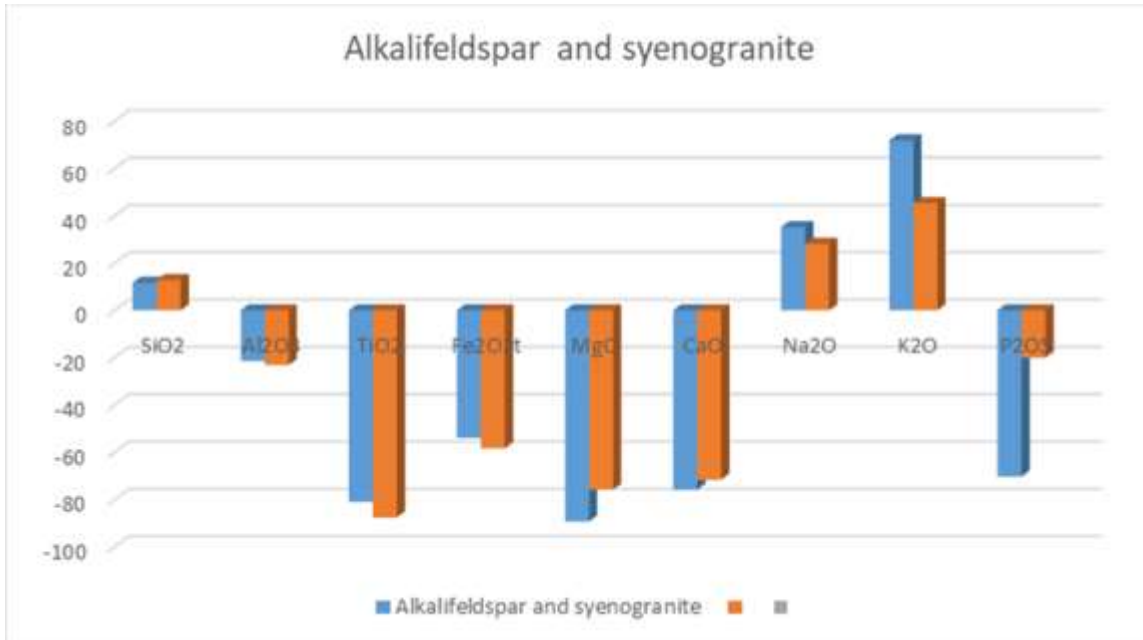
**Table 1:** Major oxides, trace elements, Rare earth elements and CIPW norms for the studied granites.

sample	Alkali Feldspar granites									Syenogranites									
	1	2	3	4	5	6	7	8	9	10	11	12	13	14	15	16	17	18	19
SiO <sub>2</sub>	73.2	73.1	74.7	73.8	73.1	74.8	75.5	75.8	75.8	75.4	74.3	74.8	76.6	74.7	74.6	75.2	76.0	75.3	74.6
TiO <sub>2</sub>	0.1	0.2	0.1	0.2	0.1	0.1	0.1	0.1	0.1	0.1	0.1	0.1	0.1	0.0	0.0	0.1	0.1	0.1	0.1
Al <sub>2</sub> O <sub>3</sub>	13.4	13.2	12.4	12.1	13.2	11.1	11.5	10.7	11.4	11.8	11.8	12.2	11.6	11.8	12.0	11.9	11.7	11.9	11.7
Fe <sub>2</sub> O <sub>3</sub>	0.9	1.2	1.0	1.5	1.6	1.4	1.2	1.4	1.6	1.2	1.4	0.9	1.4	1.3	1.8	1.3	1.3	1.5	1.4
FeO	0.8	1.0	0.8	1.2	1.3	1.1	0.8	0.9	0.4	0.4	1.0	1.2	0.4	0.4	0.9	0.7	0.6	0.5	0.8
Fe <sub>3</sub> O <sub>4</sub>	1.8	2.2	1.8	2.8	3.1	2.6	2.1	2.4	2.1	1.6	2.5	2.2	1.9	1.7	2.8	2.0	2.0	2.0	2.3
MgO	0.2	0.2	0.1	0.2	0.2	0.3	0.5	0.3	0.4	0.4	0.9	0.5	0.5	0.6	0.6	0.6	0.4	0.7	0.8
CaO	1.1	0.7	0.6	1.0	1.2	0.8	1.1	0.6	0.7	1.0	1.3	1.1	1.0	1.0	0.9	1.1	0.8	0.9	1.1
Na <sub>2</sub> O	4.7	4.2	4.5	4.5	4.4	4.4	4.3	4.4	4.4	4.2	4.0	4.2	4.2	4.3	4.2	4.3	4.2	4.2	4.1
K <sub>2</sub> O	4.7	5.4	5.2	4.9	4.7	4.8	4.5	4.6	4.5	4.1	4.1	4.2	4.0	4.2	4.0	4.1	4.0	4.0	4.0
P <sub>2</sub> O <sub>5</sub>	0.0	0.0	0.0	0.0	0.0	0.1	0.1	0.1	0.1	0.2	0.1	0.1	0.1	0.1	0.2	0.1	0.1	0.1	0.1
H <sub>2</sub> O <sup>+</sup>	0.6	0.7	0.5	0.6	0.5	0.9	1.4	0.1	1.4	1.1	0.6	0.9	1.0	1.3	0.5	1.2	0.8	1.1	1.0
Total	101.7	102.1	101.7	102.6	103.3	102.2	103.2	101.3	102.8	101.5	102.0	102.3	102.7	101.4	102.4	102.4	102.0	102.1	101.9
Rb	443.0	470.0	463.7	507.9	594.4	490.0	515.0	530.0	520.0	385.0	332.0	467.0	233.0	189.0	382.0	363.0	485.0	367.0	443.0
Ba	376.0	308.0	334.0	219.0	237.0	322.0	303.0	317.0	739.0	106.0	97.0	114.0	416.0	573.0	91.0	103.0	109.0	106.0	121.0
Sr	92.0	81.0	92.0	76.0	83.0	93.0	54.0	89.0	73.0	38.0	34.0	29.0	158.0	167.0	11.0	37.0	14.0	25.0	29.0
Zr	202.0	236.0	220.0	210.0	357.0	199.0	187.0	206.0	85.0	108.0	106.0	119.0	118.0	148.0	101.0	96.0	95.0	93.0	108.0
Hf	13.2	9.0	10.2	9.7	13.7	9.5	8.9	9.8	4.1	5.1	5.1	5.7	5.6	7.1	4.8	4.6	4.5	4.4	5.1
Nb	95.0	91.0	109.0	91.4	87.0	83.0	74.0	87.0	78.0	29.0	19.0	40.0	18.0	17.0	34.0	24.0	28.0	29.0	37.0
Ta	8.2	8.8	9.4	8.6	9.0	8.5	9.0	8.0	7.4	2.8	1.8	3.9	1.7	1.6	3.2	2.3	2.7	2.8	3.5
Ga	31.5	31.2	32.7	32.6	33.6	33.1	34.1	32.7	29.0	22.0	24.0	28.0	30.0	27.0	26.0	28.0	25.0	26.0	28.0
Y	48.3	60.2	69.2	57.3	58.3	60.0	59.0	55.0	58.0	57.0	51.0	57.0	53.0	53.0	60.0	55.0	60.0	54.0	61.0
Pb	18.8	19.9	52.0	42.2	44.4	20.0	47.0	17.0	21.0	25.0	34.0	88.0	73.0	40.0	33.0	44.0	42.0	41.0	81.0
Zn	31.7	41.5	81.9	61.0	77.1	20.0	23.0	222.0	10.0	79.0	95.0	77.0	26.0	46.0	49.0	55.0	52.0	68.0	85.0
U	3.6	6.2	24.8	15.7	20.2	45.0	138.0	216.0	17.0	112.0	63.0	52.0	76.0	106.0	51.0	48.0	52.0	39.0	368.0
Th	27.4	30.7	47.4	42.0	34.9	29.0	84.0	96.0	5.0	82.0	50.0	21.0	54.0	76.0	55.0	18.0	16.0	13.0	112.0
La	36.5	38.1	37.2	35.3	39.7	40.2	36.5	35.4	36.1	30.0	29.0	31.0	31.0	31.0	28.0	26.0	29.0	28.0	27.0
Ce	68.9	74.6	66.5	67.5	68.3	62.3	70.1	66.4	78.2	56.0	57.0	55.0	64.0	66.0	64.0	61.0	62.0	63.0	60.0
Pr	7.5	8.6	8.1	7.2	8.2	7.2	7.5	6.8	8.8	6.5	6.8	7.1	7.2	7.2	6.9	6.9	6.8	6.8	6.7
Nd	33.4	30.9	32.2	28.9	34.2	29.4	34.1	31.0	34.1	29.6	29.4	32.0	29.8	29.4	28.9	30.1	29.9	29.5	29.7
Sm	5.4	6.1	5.2	5.2	5.5	6.1	5.9	5.3	6.2	4.8	4.7	4.6	5.1	5.0	5.1	5.1	4.9	4.8	4.9
Eu	0.3	0.4	0.3	0.2	0.3	0.4	0.4	0.2	0.3	0.5	0.5	0.4	0.5	0.5	0.5	0.5	0.5	0.5	0.5
Gd	6.1	5.7	6.7	6.4	6.0	6.8	7.0	6.1	6.4	4.8	4.7	5.1	4.9	4.9	5.1	4.7	4.9	4.8	4.9
Tb	1.2	1.1	1.6	1.2	1.2	1.1	1.3	1.4	1.5	1.1	1.0	1.1	1.1	1.0	1.1	1.0	1.0	1.2	1.1
Dy	8.1	7.3	8.8	9.4	8.4	7.9	8.2	9.2	9.6	6.9	7.2	6.9	6.8	6.8	7.1	7.2	7.1	6.9	7.1
Hm	1.3	1.4	1.6	1.4	1.6	1.5	1.6	1.5	1.5	1.3	1.4	1.2	1.2	1.2	1.1	1.1	1.1	1.2	1.3
Tm	0.6	0.7	0.9	0.8	0.8	0.8	0.8	0.8	0.8	0.7	0.7	0.6	0.7	0.6	0.7	0.7	0.7	0.6	0.6
Yb	3.1	2.9	3.1	3.5	3.8	2.8	3.2	3.6	3.4	2.8	2.8	2.4	2.8	2.7	2.7	2.8	2.6	2.8	2.8
Lu	0.3	0.3	0.4	0.3	0.4	0.3	0.3	0.3	0.3	0.3	0.3	0.2	0.3	0.2	0.3	0.3	0.2	0.2	0.2

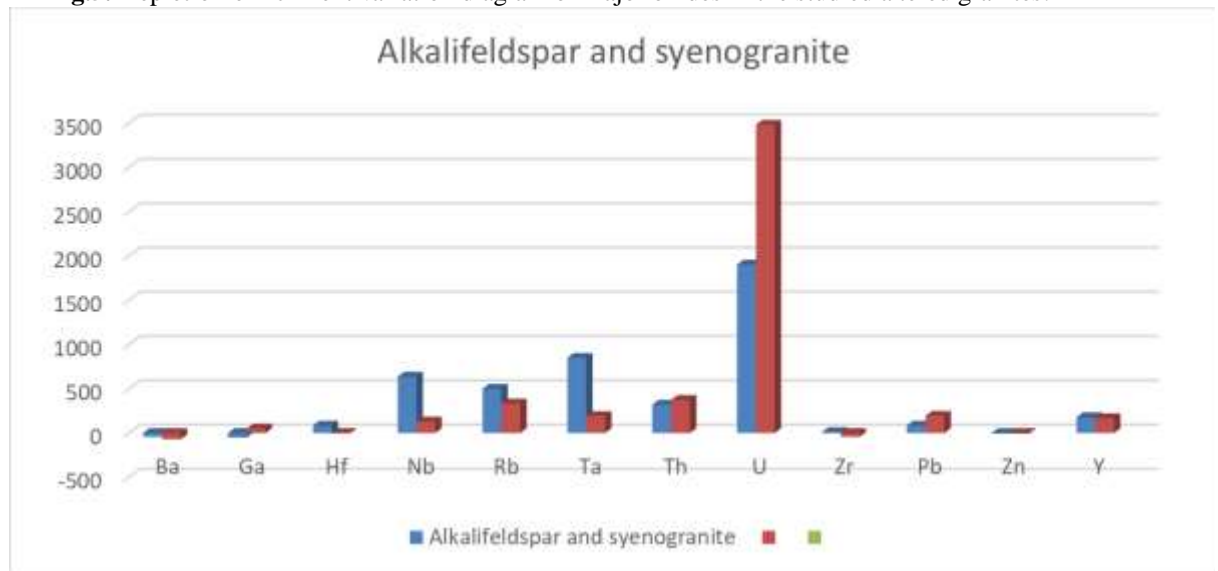
La/Y	0.76	0.63	0.54	0.62	0.68	0.67	0.62	0.64	0.62	0.53	0.57	0.54	0.58	0.58	0.47	0.47	0.48	0.52	0.44
La/Yb <sub>n</sub>	8.0	8.9	8.1	6.8	7.1	8.8	7.7	6.6	7.2	8.8	7.0	8.7	7.5	7.8	9.1	6.3	7.5	6.8	6.5
La/Sm <sub>n</sub>	4.3	3.9	4.5	4.3	4.5	3.8	3.9	4.2	3.7	4.8	3.9	4.2	3.8	3.9	4.5	3.2	3.7	3.7	3.5
Gd/Yb <sub>n</sub>	1.6	1.6	1.7	1.5	1.3	2.0	1.8	1.4	1.5	1.4	1.4	1.7	1.4	1.5	1.5	1.4	1.5	1.4	1.4
Sr/Eu	306.67	202.50	306.67	380.00	276.67	232.50	135.00	445.00	243.33	76.00	68.00	72.50	316.00	334.00	22.00	74.00	28.00	50.00	58.00
Eu/Sm	0.056	0.066	0.058	0.038	0.055	0.066	0.068	0.038	0.048	0.104	0.106	0.087	0.098	0.100	0.098	0.098	0.102	0.104	0.102
Y/Ho	37.15	43.00	43.25	40.93	36.44	40.00	36.88	36.67	38.67	43.85	36.43	47.50	44.17	44.17	50.00	50.00	54.55	45.00	46.92
REE	136.2	145.2	140.9	137.3	144.4	132.2	146.2	137.9	155.9	119.9	120.7	121	128.5	129.58	127.8	125.7	126.2	126.2	123.9
LREE	115.5	120.6	112.3	109	116.5	105.4	118	109.7	127.6	97.4	98.4	99.1	106.6	108.1	105.4	103.6	104.1	104.6	101.8
HREE	20.7	24.6	28.6	28.3	27.9	26.8	28.2	28.2	28.3	22.5	22.3	21.9	21.9	21.48	22.4	22.1	22.1	21.6	22.1
LREE/HREE	5.58	4.90	3.93	3.85	4.18	3.93	4.18	3.89	4.51	4.33	4.41	4.53	4.87	5.03	4.71	4.69	4.71	4.84	4.61
Ce/Ce*	0.93	1.00	0.9	0.98	0.86	0.93	0.94	0.94	1.06	0.93	0.94	0.84	1.00	1.04	0.93	1.07	1.01	1.06	1.03
Eu/Eu*	0.16	0.20	0.16	0.11	0.16	0.19	0.19	0.11	0.14	0.32	0.32	0.25	0.30	0.31	0.30	0.31	0.31	0.32	0.31
Zr/Hf	15.30	26.22	21.57	21.65	26.06	20.95	21.01	21.02	20.73	21.18	20.78	20.88	21.07	20.85	21.04	20.87	21.11	21.14	21.18
Nb/Ta	11.59	10.34	11.60	10.63	9.67	9.76	8.22	10.88	10.54	10.36	10.56	10.26	10.59	10.63	10.63	10.43	10.37	10.36	10.57
U/Th	0.13	0.20	0.52	0.37	0.58	1.55	1.64	2.25	3.40	1.37	1.26	2.48	1.41	1.39	0.93	2.67	3.25	3.00	3.29
Ba/Sr	4.09	3.80	3.63	2.88	2.86	3.46	5.61	3.56	10.12	2.79	2.85	3.93	2.63	3.43	8.27	2.78	7.79	4.24	4.17
Ba/Rb	0.85	0.66	0.72	0.43	0.40	0.66	0.59	0.60	1.42	0.28	0.29	0.24	1.79	3.03	0.24	0.28	0.22	0.29	0.27
Rb/Sr	2.19	1.99	2.11	2.42	1.66	2.46	2.75	2.57	6.12	3.56	3.13	3.92	1.97	1.28	3.78	3.78	5.11	3.95	4.10



t <sub>1</sub>	0.92	1.04	0.95	0.97	0.91	0.92	0.92	0.9	1.05	0.92	0.95	0.89	1	1.02	0.92	1.03	0.98	1.02	1
t <sub>3</sub>	1.2	1.09	1.25	1.22	1.11	1.2	1.06	1.29	1.33	1.2	1.14	1.21	1.23	1.17	1.2	1.28	1.25	1.3	1.2
TE <sub>1,3</sub>	1.05	1.07	1.09	1.09	1	1.05	0.99	1.08	1.19	1.05	1.04	1.04	1.11	1.09	1.05	1.15	1.11	1.15	1.1
t <sub>4</sub>	1.22	1.18	1.17	1.38	1.2	1.22	1.26	1.4	1.42	1.22	1.29	1.33	1.31	1.46	1.22	1.28	1.47	1.52	1.48
TE <sub>1,4</sub>	1.06	1.11	1.05	1.16	1.04	1.06	1.07	1.12	1.23	1.06	1.11	1.08	1.14	1.22	1.06	1.15	1.2	1.24	1.22



**Fig.5:** Depletion-enrichment variation diagram of major oxides in the studied altered granites.



**Fig.6 :** Depletion-enrichment variation diagram of minor elements in the studied altered granites .

deep anoxic waters rich in organic materials, and/or mixing with shallower oxic seawater before deposition [52].

### Isovalent parameters.

The tetrad effect is often accompanied by other modified geochemical behavior of many trace elements, which is termed by [21] as non-CHARAC behavior. Such behavior occurs typically in highly evolved magmatic systems which are rich in H<sub>2</sub>O, CO<sub>2</sub> and elements such as Li, B, F and/or Cl, and which may be regarded as transitional between a pure silicate melt and an aqueous fluid (e.g., [21,53, 54]).

Hf and Zr are similar in geochemical behavior, resulting in a small range of ratios in geological materials [55]. According to [56], granites with Zr/Hf ratio (< 20) are affected by strong magmatic hydrothermal alteration. This ratio shifts towards smaller values with increasing evolution of silicate melt. In most igneous rocks, Zr/Hf ratios fall in a narrow range of 33–40 and deviation from the range is related to metasomatism or intense fractionation of accessory minerals.

The Zr/Hf ratios determined for the alkali feldspar granites (15.30–26.22) and the syenogranites (22.92–29.7318) are lower than the norm for geological materials, suggesting the effect of later hydrothermal solutions.

The chondritic value of Y/Ho ratio is 28.8 [21]. The studied samples returned Y/Ho ratios higher than the chondritic value: Y/Ho ratio of the alkali feldspar was 36.44–43.25 and the syenogranites 36.43–54.55. These higher ratios suggest complexation with fluorine. Complexation with bicarbonate causes Y/Ho values 28. It has been reported that Y/Ho ratio would be discrepant from the chondritic value (Y/Ho = 28.8) for samples showing a

tetrad effect [57,21,58] stated that Y/Ho ratio shows values higher than the chondritic values for samples having W-type tetrad effect. This is the case of this study, where Y/Ho ratio >28 in the two rock types. Y/Ho ratios for the crust, mantle and high-temperature hydrothermal fluids are within the range of ~26–28, whereas this ratio for seawater and marine sediments increases to ~47 [54,30]. The main reason for this increase was interpreted to be preferential scavenging of Ho by Mn-oxyhydroxides [21].

The chondritic value of Nb/Ta is  $17.6 \pm 1$  according to [31]; the studied rock varieties had Nb/Ta ratios lower than the chondritic: Nb/Ta of the alkalifeldspar granite samples was 8.22–11.60 and the syenogranite samples 10.26–10.63.

Rb/Sr ratio increases with differentiation; this is due to Sr being depleted in the liquid magma by crystallization of feldspar, while Rb is enriched. This ratio ranged from 1.66 to 6.12 in the alkalifeldspar granite samples and from 1.28 to 5.11 in the syenogranite samples.

This is probably due to the effect of albitization accompanied by Sr enrichment.

The relatively high average of uranium and thorium contents in the studied alkali feldspar (64.19–45.22) and syenogranites (114.50–51.83, respectively), comparing with the crustal values of 1.80 ppm U and 7.20 ppm Th [59] illustrate that Magal Gebriel granites are high uranium high thorium rocks. These may be resulted from the newly formed mineral phases which are characterized by non-chondritic (or non-CHARAC) ratios of the geochemical twins, where they contain higher amounts of lighter partners such as Y and Th over Ho and U [60]. U/Th average of the two granitic rocks are 1.29 and 2.11, respectively) in alkali feldspar and syenogranites, which are higher than the U/Th chondritic value (0.33), suggesting the effect of later hydrothermal processes in radionuclides mineralization.

### Rare Earth Elements.

The average of the total REE content of the studied syeno- and alkalifeldspar granite (av.  $\Sigma$ REE = 142.21 & 124.91 ppm, respectively) are lower than that of the worldwide granite ( $\Sigma$ REE = 250–270 ppm) as given by [45,61]. The depletion of REEs could be attributed to hydrothermal alteration by severe acidic solution as indicated in the values of La/Y ratios of these rocks, which are all lower than unity. There is notable decrease in the REE contents from syeno- to alkalifeldspar granite, where  $\Sigma$ REE ranges are (132.20–155.90) & (119.90–129.58) ppm in syeno- and alkalifeldspar granite, respectively (Table 1), but  $\Sigma$ LREE in syeno- and alkali feldspar granite (105.40–127.60 ppm) & (97.40–108.10) are higher than  $\Sigma$ HREE (20.70–28.60) and (21.48–22.50 ppm) and  $\Sigma$ LREE/ $\Sigma$ HREE (3.95–5.58) & (4.33–5.03), respectively. The fractionation of the REE in syeno- and alkali feldspar granite are low and nearly identical in the rock types where La/Yb ratio ranges in syenogranites are (6.60–8.90) and in alkali feldspar granite (6.30–9.10). La/Yb is well-known to range between (30 and 80) for metaluminous or slightly peraluminous granites (Fig.7&8). The LREE (La/Sm 3.7–4.5) for syenogranites and (3.20–4.80) for alkalifeldspar granite whereas the HREE (Gd/Yb 1.30 to 2.00) for syenogranites and (1.4–1.7) for alkalifeldspar granite, which are slightly fractionated. A negative Eu anomaly characterizes these granites, where Eu/Eu\* (0.11–0.20) for syenogranites and (0.25–0.30) for alkalifeldspar. The fractionation among Eu and neighboring REE (Sm and Gd) with the tetrad effect possibly leads to a decrease in the magnitude of the negative Eu anomaly [62].

The REE tetrad effect is characterized by a kinked pattern, especially in highly evolved granitic rocks. Both M-type and W-type REE tetrad effects can be observed in a peraluminous melt, with the former in the residual melt phase and the latter in the fluid [63]. An MW-type of REE tetrad effect has been recorded previously in China [64 :66, 62].

The REE pattern kinks are characterized by prominent convex and concave tetrads and negative Eu anomalies. Visual inspection suggests that the third and fourth tetrads in most samples are more prominent than the first. The second tetrad is comparatively difficult to recognize due to the anomalous behavior

of Eu and the fact that Pm does not occur in nature. Figures and Table show the strong M-type tetrad effect in the third and fourth tetrad and strong W-type tetrad effect in the first tetrad observed in samples of the syenogranite. MW-type tetrad effect may result from the interaction of aqueous liquids with alkaline rocks [67].

In Kab Amiri granite, CED, Egypt, [40] revised the convex (M-type) T1 to concave (Wtype) T3 due to changes in the physico-chemical conditions that prevailed during alkali-metasomatism. [68] stated that the peculiar MW-type tetrad effect might be an indicator of Au mineralization of reworked plutons and this vision could be applied in the study area.

## Conclusions

The study area comprises volcano sedimentary succession (metasediment and metavolcanics) intruded by granitoid rocks. The younger granites occupy central, northeastern and northwestern parts of the area, they form moderate to high outcrops and have sharp intrusive contacts with the surrounding metavolcanics. Petrographically, Syeno- and alkali-feldspar granites are mainly composed of quartz, alkali feldspar, plagioclase, biotite and muscovite as essential minerals, fluorite, zircon, allanite, titanite, monazite, uranophane and iron oxides as accessories. Geochemically, these rocks are affected by hydrothermal alteration followed by water-rich solution, these water-rock interaction lead to conjugate M-W tetrad phenomena and provable gold mineralization. All these physico-chemical conditions were confirmed by the non-chondritic values of isovalents. Alteration processes were accompanied with increments and decrements' in major, trace and rare earth elements due to formation of new mineral associations. All samples of the alkali-feldspar and syenogranite samples have La/Y ratios less than unity, suggesting the prevailing of acidic conditions in the depositional environment.

## References

- [1] A. Sabet, B. LM, R. AM, and A. LK, 1976. Geologic structure and laws of localization of tantalum mineralization at the Nuweibi deposit.
- [2] R. L. Linnen, M. Van Lichtervelde, and P. J. E. Černý, Granitic pegmatites as sources of strategic metals. 8(4):p. 275-280, 2012.
- [3] I. Lambert, S. Jaireth, A. McKay, and Y. J. A. n. Miezitis, 2005. Why Australia has so much uranium. 807-10.
- [4] M. J. B. d. I. S. G. d. F., 2014. Cuney, Felsic magmatism and uranium deposits. 185(2):p. 75-92,
- [5] G. Saleh and M. J. o. Kamar, 2018. Geochemical Characteristics and Radioactive Elements Estimation along Trenches of Um Ara area, South Eastern Desert, Egypt. Geoinfor Geostat: An Overview 6: 2. 162.
- [6] IAEA, 2012. World distribution of uranium deposits (UDEPO) with uranium deposit classification. Int At Energy Agency.
- [7] M. E. Ibrahim, 1996. Petrochemical investigations on Magal Gebriel uraniumiferous granites, South Eastern Desert, Egypt. Proc. Egypt. Acad. Sci., 46, 587-601.,
- [8] S. S. Farag, 1990. Geology and radioactivity of Magal Gebriel area, Southeast Aswan, Egypt. Al-Azhar Univ.: Egypt., p. 141p.
- [9] A. F. Kamel, 1993. Comparative study on two radioactive exposures in Southeastern Desert, Egypt. Geoscientific Reserch in Northeast Africa, ed. U.T.H. Schandelmeier. Balkema, Rotterdam. 793.
- [10] M. G. Mahfouz, 1998. Geochemical and technological studies for some mineralized granite in Magal Gebriel area, South Eastern Desert, Egypt. Fac. Sci., Ain Shams Univ.,: Egypt. p. 152p.,
- [11] S.M. El Shazly and H. A. Hegazy, 2000. Geochemistry and petrogenesis of a late proterozoic volcanic sequence in the Magal Gebriel area, South Eastern Desert, Egypt. Qatar Univ. Sci. J., 20,181-195.
- [12] H. Sehsah, 2017. CRUSTAL EVOLUTION OF ABU SWAYEL AREA, SOUTH EASTERN DESERT, EGYPT, in Geology Dept., Damietta Univ.: Faculty of Science., p. 198.
- [13] Karakaya, N., 2009. REE and HFS element behavior in the alteration facies of the Erenler Dağı Volcanics (Konya, Turkey) and kaolinite occurrence. J. Geochem. Explor. 101, 185–208.
- [14] Jiang, N., Sun, S., Chu, X., Mizuta, T., Ishiyama, D., 2003. Mobilization and enrichment of high-field strength elements during late- and post-magmatic processes in the Shuiquangou syenitic complex, Northern China. Chem. Geol. 200, 117–128.
- [15] Karadag, M.M., Kupeli, S., Aryk, F., Ayhan, A., Zedef, V., and Doyen, A., 2009. Rare earth element (REE) geochemistry and genetic implications of the Mortas bauxite deposit (Seydisehir/Konya-Southern Turkey). Chemie Der Erde, 69: 143– 159.
- [16] Fulignati, P., Gioncada A. and Sbrana A., 1999. Rare earth element (REE) behaviour in the alteration facies of the active magmatic-hydrothermal system of Vulcano (Aeolian Islands, Italy). Journal of Volcanology and Geothermal Research, 88: 325–342.
- [17] Salvi, S., and Williams-Jones, A.E., 1996. The role of hydrothermal processes in concentrating high-field strength elements in the Strange Lake peralkaline complex, northeastern Canada Volume 60, Issue 11, Pages 1917-1932
- [18] Braun, J.-J., Pagel, M., Muller, J.-P., Bilong, P., Michard, A., Guillet, B., 1990. Cerium anomalies in lateritic profiles. Geochim. Cosmochim. Acta 54, 781–795
- [19] Uysal and Golding, 2003; Rare earth element fractionation in authigenic illite-smectite from Late Permian clastic rocks, Bowen Basin, Australia: Implications for physico-chemical environments of fluids during illitization. Chemical Geology 193(3–4): 167–179.
- [20] S. Pati<sup>no</sup>1,2,3, J. Lloyd<sup>2</sup>, R. Paiva<sup>4</sup>, C. A. Quesada<sup>2,5</sup>, T. R. Baker<sup>2</sup>, A. J. B 2003.. Branch xylem density variations across Amazonia ,Biogeosciences Discuss., 5,
- [21] Bau, M., 1996. Controls on the fractionation of isoivalent trace elements in magmatic and aqueous systems: evidence from Y/Ho, Zr/Hf, and lanthanide tetrad effect. Contrib. Mineral. Petrol. 123, 323–333.

- [22] Fidelis, i. & siekieRski, s. 1966. The regularities in stabil-ity constants of some rare earth complexes. – Journal ofInorganic and Nuclear Chemistry, 28: 185-18
- [23] PePPaRd, d.F., mason, g.w. & lewey, s. 1969. A tetrad effect in the liquid – liquid extraction ordering of lantha-nide (III). – Journal of Inorganic and Nuclear Chemistry,31: 2271-227
- [24] Takahashi, y., chaTellieR, X., haTToRid, k.h., kaToe, k. &FoRTin, d. 2005.Adsorption of rare earth elements ontobacterial cell walls and its implication for REE sorptiononto natural microbial mats. – Chemical Geology, 219:53-67.
- [25] NakamuRa, k., moRishiT, T., chang, q., neo, n. & kumagai,h. 2007. Discovery of lanthanide tetrad effect in an oceanic plagiogranite from an Ocean Core Complex at the Central Indian Ridge 25° S. – Geochemical Journal,41: 135-140.
- [26] PéRez-lóPez, R., delgado, J., miguel nieTo, J. & máRquez-gaRcía, B. 2010.Rare earth element geochemistry of sulphide weathering in the São Domingos mine area(Iberian Pyrite Belt): A proxy for fluid-rock interactionand ancient mining pollution. – Chemical Geology, 276:29-40.
- [27] PeReTyazhko, i.s. & savina, e.a. 2010.Tetrad effects in the rare earth element patterns of granitoid rocks as an indicator of fluoride silicate liquid immiscibility in mag-matic systems. – Petrology, 18: 514-543.
- [28] Pérez-Soba & Villaseca .2010.Petrogenesis of highly fractionated I-type peraluminous granites: LaPedriza pluton (Spanish Central System). – GeologicaActa, 8:131-149.
- [29] Bishady, a.m., el-sheRiF, a.m. & daRwish, m.e. 2016.Petrological and Geochemical Constraints on the Evolu-tion of El-Kahfa Alkaline Ring Complex, South EasternDesert, Egypt. – Journal of Geological Resource andEngineering, 6: 283-304.
- [30] Abedini, A., Azizi, M.R., and Calagar, A.A., 2018. The Lanthanide Tetrad Effect in Argillic Alteration: An Example from the Jizvan District, Northern Iran. Acta Geologica Sinica, 92(4): 1468–1485.
- [31] Jahn, B.m., wu, F., caPdevila, R., maRTineau, F., zhao, z.& wang, y. 2001.Highly evolved juvenile granites withtetrad REE patterns: The Woduhe and Baerzhe granitesfrom the Great Xing'an Mountains in NE China. – Li-thos, 59: 171-198
- [32] PayTan, a. & mclaughlin, k. 2007. The Oceanic Phos-phorus Cycle. – Chemical Review, 107: 563-576.
- [33] Jiang, s.y., zhao, h.X. & chen, y.q. 2007. Trace and RareEarth Element Geochemistry of Phosphate Nodules fromthe Lower Cambrian Black Shale Sequence in the MufuMountain of Nanjing, Jiangsu Province, China. – Chemi-cal Geology, 244: 584-604.
- [34] GoYne, k.w., BRanTley, s.l.c. & choRoveR, J. (2010).Rare earth element release from phosphate minerals in the presence of organic acids. – Chemical Geology, 278:1-14.
- [35] Zhu, B., Jiang, s.y. & yang, J.h. 2014. Rare Earth Elementand Sr-Nd Isotope Geochemistry of Phosphate Nodulesfrom the Lower Cambrian Niutitang formation, NWHunan Province, South China. – Palaeogeography, Pal-aeoclimatology, Palaeoecology, 398: 132-143
- [36] Xin, h., Jiang, s., yang, J., wu, h. & Pi, d. 2016. Rareearth element geochemistry of phosphatic rocks in Neo-proterozoic Ediacaran Doushantuo Formation in Hushansection from the Yangtze Gorges Area, South China. –Journal of Earth Science, 27 (2): 204-210.
- [37] Xin, h., Jiang, s.y. & yang, J.h. 2015.Rare Earth Elementand Sr-Nd Isotope Geochemistry of phosphatic rocks inNeoproterozoic Ediacaran Doushantuo Formation inZhangcunping section from Western Hubei Province,South China. – Palaeogeography, Palaeoclimatology,Palaeoecology, 440: 712-724.
- [38] J. J. Hemly and J. W.R., 1964.Chemical aspects of hydrothermal alteration with emphasis on hydrogen metasomatism. [J]. Econ. Geol., 59:538–351,
- [39] S. J.S. and S. W.E., 1990. The effect of temperature on metal mobility in subsea floor hydrothermal systems: Constraints from basalt alteration experiments. [J]. Earth Planet. Sci. Lett., 101,388–403.
- [40] Rudnick RL, Gao S (2003) Composition of the Continental Crust. In: Holland HD, Turekian KK (eds) Treatise on Geochemistry, vol 3. Elsevier, Oxford, p 659.
- [41] El Feky M, Mohammed, H, El-Shabasy, A., Ahmed, M, Abdel-Monem, Y and Mira, H 2021. Mobilisation of radionuclides during uranium and gold processing of granitic rock at El-Missikat area, central Eastern Desert, Egypt. International Journal of Environmental Analytical Chemistry ISSN: (Print) (Online) Journal homepage: <https://www.tandfonline.com/loi/geac20>.
- [42] Maksimovic, Z., Pantó, G.Y., 1991. Contribution to the geochemistry of the rare earth elements in the karst-bauxite deposits of Yugoslavia and Greece. Geoderma 51, 93–109.
- [43] Crinci, J., Jurkovic, I., 1990. Rare earth elements in Triassic bauxites of Croatia Yugoslavia. In: Travaux. 19. pp. 239–248.
- [44] Henderson, P., 1984. Rare Earth Element Geochemistry. Elsevier Scientific, Amsterdam.
- [45] Herrman, A. G. 1970. Yttrium and lanthanides: in Wedepohl (ed.) Handbook of Geochemistry, Springer-Verlag, New York, pp. 39-57.
- [46] Dill, H.G., Luna, L.I., Nolte, N., and Hansen, B.T., 2016. Chemical, isotopic and mineralogical characteristics of volcanogenic epithermal fluorite deposits on the PermoMesozoic foreland of the Andean volcanic arc in Patagonia (Argentina). Geochemistry, 76: 275–297.
- [47] Kraemer, D., Tepe, N., Pourret, O., and Bau, M., 2017. Negative cerium anomalies in manganese (hydr)oxide precipitates due to cerium oxidation in the presence of dissolved siderophores. Geochimica et Cosmochimica Acta, 196: 197–208.
- [48] Constantopoulos J ,1988. Fluid inclusions and rare earth element geochemistry of fluorite from South-Central Idaho. Econ Geol 83(3):626–636.
- [49] Mongelli, G., Boni, M., Buccione, R., and Sinisi, R., 2014. Geochemistry of the Apulian karst bauxites (southern Italy): chemical fractionation and parental affinities. Ore Geology Review, 63: 9–21.
- [50] Hannigan, R., Dorval, E., and Jones, C., 2010. The rare earth element chemistry of estuarine surface sediments in the Chesapeake Bay. Chemical Geology, 272: 20–30.
- [51] Schwinn, G., and Markl, G., 2005. REE systematics in hydrothermal fluorite. Chemical Geology, 216: 235–248.
- [52] Khan, s.a., Khan, k.F. & daR, s.a. 2016.REE geochem-istry of Early Cambrian phosphorites of Masrana and Kimoi blocks, Uttarakhnad, India. – Arabian Journal of Geosciences, 9 (456): 1-10 .
- [53] London, D., 1987. Internal differentiation of rare-element pegmatites: effect of boron, phosphorus and fluorine. Geochim. Cosmochim. Acta 51, 403–420.

- [54] Gadd, m.g., layTon-maTThews, d. & PeTeR, J.m. 2016. Non-hydrothermal origin of apatite in SEDEX mineralization and host rocks of the Howard's Pass district, Yukon, Canada. – *American Mineralogist*, 101: 1061-107
- [55] J. Dostal, A.K. Chatterjee (2000). Contrasting behaviour of Nb/Ta and Zr/Hf ratios in a peraluminous granitic pluton (Nova Scotia, Canada) *Chemical Geology Volume 163, Issues 1–4, Pages 207-218*.
- [56] IRBeR, w. 1999. The lanthanide tetrad effect and its correlation with K/Rb, Eu/Eu\*, Sr/Eu, Y/Ho, and Zr/Hf of evolving peraluminous granite suites. – *Geochimica et Cosmochimica Acta*, 63: 489-508.
- [57] Zhang et al., 1994. The gene for biotin synthase from *Saccharomyces cerevisiae*: cloning, sequencing, and complementation of *Escherichia coli* strains lacking biotin synthase. *Arch Biochem Biophys* 309(1):29-35
- [58] Takahashi, y., yoshida, h., saTo, n., hama, k., yusa, y. & shimizu, h. 2002. W- and M-type tetrad effects in REE patterns for water-rock systems in the Tono uranium deposit, central Japan. – *Chemical Geology*, 184: 311-335.
- [59] Mason B, Moore CB., 1991. *Principles of Geochemistry*. 4th edition, Wiley Eastern Limited, 350 p.
- [60] El Mezayen, A, Ibrahim, E, El-Feky, M, Omar, S, El-Shabasy, A and Taala, S., 2020. Physicochemical conditions controlling the radionuclides mobilisation in various granitic environments, *International J. of Environmental analytical chemistry*.
- [61] El Feky, M, El Mowafy, A and Abdel Warith, A., 2011. Mineralogy, geochemistry, radioactivity and environmental impacts of Gabal Marwa granites, southeastern Sinai, Egypt. *China J. Geochem.*, 30, 175–186.
- [62] Mahdy AI, El-Kammar AM., 2003. Geochemical Partitioning of Isovalent and Tetrad Effect of REE Associating Episyntization of Kab Amiri Granites, Central Eastern Desert of Egypt. pp.111–125. 5th In. *Conf. of Geology of Middle East Cairo Egypt*
- [63] SALLAM, Osama R., MIRA Hamed I. El TOHAMY, Amira M. and ABBAS Abd Elhadi A., 2021. Mineralogy and Geochemistry of Uraniferous Sandstones in Fault Zone, Wadi El Sahu Area, Southwestern Sinai, Egypt: Implications for Provenance, Weathering and Tectonic Setting *Acta Geologica Sinica (English Edition)*, 95(3): 830–845.
- [64] Masuda, A., Kawakami, O., Dohmoto, Y., and Takenaka, T., 1987. Lanthanide tetrad effects in nature: two mutually opposite types, W and M. *Geochemical Journal*, 21: 119–124.
- [65] Zhao, Z.H., Bao, Z.W., and Lee Seung, G.U., 2008. A composite M- with W-type of REE tetrad effect in a north China alkaline complex. *Geochimica et Cosmochimica Acta*, 72: 11095.
- [66] Cao, m.J., zhou, q.F., qin, k.z., Tang, d.m. & evans, n.J. 2013. The tetrad effect and geochemistry of apatite from the Altay Koktokay No. 3 pegmatite, Xinjiang, China: implications for pegmatite petrogenesis. – *Mineralogy and Petrology*, 107: 985-1000  
(2) (PDF) Rare earth element geochemistry and tetrad effects of the Dalir phosphatic shales, northern Iran. Available from:
- [67] Abedini, A., Rezaei Azizi, M., Calagari, A.A., Cheshmehsari, M., 2017. Rare earth element geochemistry and tetrad effects of the Dalir phosphatic shales, northern Iran. *N. J. Geol. Paläont. Abh.* 286, 169–188.
- [68] Zhao, Z. H., Bao, Z. W., and Qiao, Y. L., 2010. A peculiar composite M- and W-type REE tetrad effect: evidence from the Shuiquangou alkaline syenite complex, Hebei Province, China. *China Science Bulletin*, 55: 2684–2696.